REVISTA CADERNO PEDAGÓGICO – Studies Publicações Ltda.
ISSN: 1983-0882

Acoustic synthesis of random wall-pressure fields from turbulent boundary layers using monopole arrays and acoustic radiation modes

Síntese acústica de campos de pressão parietal de camadas limite turbulentas por meio de arranjos de monopolos e modos de radiação acústica

Síntesis acústica de campos de presión parietal de capas límite turbulentas mediante arreglos de monopolos y modos de radiación acústica

DOI: 10.54033/cadpedv22n13-024

Originals received: 9/29/2025
Acceptance for publication: 10/22/2025

Clinton André Merlo
Doctor in Mechanical Engineering
Institution: Universidade Federal de Itajubá (UNIFEI)
Address: Itabira, Minas Gerais, Brazil
E-mail: clintonmerlo@unifei.edu.br

Otávio Lage Dias
Graduate in Computer Engineering
Institution: Universidade Federal de Itajubá (UNIFEI)
Address: Itabira, Minas Gerais, Brazil
E-mail: d2023011241@unifei.edu.br

Rogério Fernandes Brito
Doctor in Mechanical Engineering
Institution: Universidade Federal de Itajubá (UNIFEI)
Address: Itabira, Minas Gerais, Brazil
E-mail: rogbrito@unifei.edu.br

ABSTRACT

This work investigates the acoustic synthesis of wall-pressure fields characteristic of turbulent boundary layers (TBL) by means of planar arrays of monopole sources with image symmetry. The empirical–statistical model proposed by Corcos was adopted to describe the spatial and spectral coherence of the target field, while the acoustic radiation was represented through the monopole array, thus avoiding the use of high-cost numerical methods. To stabilize the inverse problem and reduce the source effort, regularization based on Acoustic Radiation Modes (ARMs) was employed. The quality of the synthesis was assessed

through metrics that quantify spectral fidelity, spatial coherence, and excitation effort. The results showed that the Least Squares (LS) method provides higher statistical fidelity to the target field but leads to amplitudes that are impractical for experimental implementations. In contrast, ARMs regularization significantly reduced the source effort—by several orders of magnitude—although with a partial loss of fidelity at higher frequencies. It is concluded that acoustic synthesis using monopole arrays constitutes a promising alternative for the reproduction of wall-pressure fields generated by TBL, providing a solid conceptual basis for future experimental implementations.

Keywords: Turbulent Boundary Layer. Acoustic Synthesis. Wall-Pressure Fields. Monopoles. Acoustic Radiation Modes.

RESUMO

Este trabalho investiga a síntese acústica de campos de pressão parietal, característicos de camadas limite turbulentas (TBL), por meio de arranjos planos de fontes monopolares com simetria por imagem. O modelo empírico-estatístico proposto por Corcos foi adotado para descrever a coerência espacial e espectral do campo alvo, enquanto a radiação foi representada pelo arranjo de monopolos, evitando o uso de métodos numéricos de alto custo. Para estabilizar o problema inverso e reduzir o esforço das fontes, empregou-se a regularização via Modos de Radiação Acústica (ARMs). A qualidade da síntese foi avaliada por métricas que quantificam a fidelidade espectral, a coerência espacial e o esforço de excitação. Os resultados mostraram que o método de Mínimos Quadrados (MQ) proporciona maior fidelidade estatística ao campo alvo, porém com amplitudes inviáveis para aplicações práticas. Em contrapartida, a regularização por ARMs reduziu o esforço das fontes em várias ordens de magnitude, embora com perda parcial de fidelidade em altas frequências. Conclui-se que a síntese acústica com arranjos de monopolos constitui uma alternativa promissora para a reprodução de campos de pressão parietal gerados por TBL, oferecendo uma base conceitual sólida para futuras implementações experimentais.

Palavras-chave: Camada Limite Turbulenta. Síntese Acústica. Campos de Pressão Parietal. Monopolos. Modos de Radiação Acústica.

RESUMEN

Este trabajo investiga la síntesis acústica de campos de presión parietal, característicos de capas límite turbulentas (TBL), mediante arreglos planos de fuentes monopolares con simetría por imagen. El modelo empírico–estadístico propuesto por Corcos fue adoptado para describir la coherencia espacial y espectral del campo objetivo, mientras que la radiación fue representada mediante el arreglo de monopolos, evitando el uso de métodos numéricos de alto costo. Para estabilizar el problema inverso y reducir el esfuerzo de las fuentes, se empleó la regularización a través de los Modos de Radiación Acústica (ARMs). La calidad de la síntesis se evaluó mediante métricas que cuantifican la fidelidad espectral, la coherencia espacial y el esfuerzo de excitación. Los resultados mostraron que el método de Mínimos Cuadrados (MQ) proporciona una mayor fidelidad estadística al campo objetivo, aunque con amplitudes

inviables para aplicaciones prácticas. En contrapartida, la regularización mediante ARMs redujo el esfuerzo de las fuentes en varias órdenes de magnitud, aunque con una pérdida parcial de fidelidad en altas frecuencias. Se concluye que la síntesis acústica con arreglos de monopolos constituye una alternativa prometedora para la reproducción de campos de presión parietal generados por TBL, ofreciendo una base conceptual sólida para futuras implementaciones experimentales.

Palabras clave: Capa Límite Turbulenta. Síntesis Acústica. Campos de Presión Parietal. Monopolos. Modos de Radiación Acústica.

1 INTRODUCTION

The study of the interaction between turbulent flows and rigid surfaces represents a central topic in aeroacoustics, with direct implications for aerospace, automotive, and structural vibroacoustic applications. In particular, wall-pressure fields generated by Turbulent Boundary Layers (TBL) exhibit a highly stochastic nature, characterized by broadband spectra and finite spatial coherence, acting as the primary excitation mechanism for panels and structural elements. The ability to reproduce such pressure fields in controlled environments is essential for assessing panel acoustic transparency, developing noise isolation and control strategies, and validating predictive models.

The acoustic synthesis of wall-pressure fields using controlled source arrays has emerged as an effective technique, extensively investigated in both experimental and numerical studies. Pioneering works by Elliott *et al*. (2005), Bravo & Maury (2006), and Maury & Bravo (2006) demonstrated that spatially correlated pressure fields can be generated from uncorrelated white-noise excitation signals, subsequently processed through shaping filters. These filters are designed to reproduce the cross-spectral density (CSD) matrix of the target field, thereby preserving its statistical coherence and spectral properties. More recently, Merlo (2023) extended this approach by applying Acoustic Radiation Mode concepts to the synthesis of diffuse fields, highlighting the technique's potential for reproducing complex, statistically consistent stochastic fields.

The classical description for the spatial coherence of TBL-induced wall pressure was established by Corcos (1964), whose model represents coherence as exponentials decaying in the streamwise and spanwise directions, modulated by a convective phase associated with a characteristic turbulence velocity. In the present work, the power spectral density (PSD) of the wall-pressure field is provided by the semi-empirical Efimtsov (1982) model, developed for high Reynolds numbers. The Efimtsov spectrum complements the Corcos coherence—capturing high-frequency decay and turbulent-scale effects—so their combination offers a robust basis for synthesizing TBL-induced pressure fields.

In this work, wall-pressure field synthesis means reproducing, in the observation plane, the second-order statistics (PSD and CSD) of the target field modeled by Corcos–Efimtsov. The approach does not attempt to reconstruct the full hydrodynamic physics of the flow; instead, it aims to statistically match the pressure field in the plane of interest.

To synthesize the acoustic field representing the modeled target field, a planar monopole array with image symmetry is employed. This configuration inherently satisfies the rigid-panel (Neumann) boundary condition, thereby avoiding full-field numerical methods such as FEM or BEM. Monopoles offer several modeling advantages, including conceptual simplicity, analytical field representations, and straightforward integration with synthesis techniques based on second-order statistical properties.

However, the synthesis formulation involves solving an inverse problem, in which the optimal source signals must be determined so that the radiated field statistically reproduces the target field. When addressed using the direct Least Squares (LS) method, this problem tends to be ill-conditioned, resulting in solutions with excessively high and physically unfeasible source amplitudes. To overcome this issue, the present work incorporates regularization via Acoustic Radiation Modes (ARMs), as proposed by Pasqual *et al*. (2010) and later applied by Merlo (2019) in the acoustic synthesis of diffuse random pressure fields. ARMs are the eigenvectors of the matrix relating source volume velocities to radiated power, forming an orthogonal basis of maximum radiation efficiency. By

restricting the synthesis space to the most efficient modes, source effort can be drastically reduced and numerical stability improved, albeit with a partial loss of fidelity at high frequencies.

The proposed methodology is evaluated using well-established metrics in statistical synthesis of wall-pressure fields, each addressing a specific aspect of target-field reproduction. The normalized mean-square error $\hat{J}_e$ quantifies overall energy deviation; the residual error $\varepsilon_{\mathbf{y}}$ measures the preservation of spatial coherence; and the root-mean-square source-velocity norm $\| \overline{\mathbf{q}^{*2}} \|$ reflects the effort required to generate the field. Joint analysis of these metrics enables an optimal balance between statistical fidelity and practical feasibility, supporting future implementations with real sources.

2 THEORETICAL BACKGROUND

The proposed methodology combines statistical modeling, acoustic synthesis of wall-pressure fields, and modal regularization to reproduce, using a reduced array of monopole sources, the random pressure field generated by a TBL over a rigid panel. The objective is for the synthesized field to preserve the statistical properties of the target field, particularly its cross-spectral density matrix.

2.1 TBL CROSS-SPECTRAL DENSITY

The target field is modeled using the classical Corcos formulation for spatial coherence, combined with a spectral law for the wall-pressure PSD. The cross-spectral density between two points is

$$S_{ww}(\omega) = S_0(\omega)\, e^{-|r_x|/L_x(\omega)}\, e^{-|r_y|/L_y(\omega)}\, e^{-j\omega r_y/U_c} \qquad (1)$$

where:

$S_0(\omega)$ is the wall-pressure power spectral density, r_x and r_y denote the spanwise and streamwise separations, respectively, and the Corcos correlation lengths follow the chosen convention $L_x = \alpha_x U_c/\omega$, $L_y = \alpha_y U_c/\omega$, $\alpha_x = 1.2$ (spanwise) and $\alpha_y = 8$ (streamwise).

The convection velocity is set to $U_c = 0.7U_\infty$ (about 70% of the free-stream velocity U_∞). For the spectral term $S_0(\omega)$, the semi-empirical Efimtsov model is adopted, which depends on the height-based Reynolds number Re_y, the Strouhal number St, the friction velocity U_τ and the wall shear stress τ_w

$$S_0(\omega) = \frac{0.01\tau_w^2\delta}{U_\tau[1+0.02\,St^{2/3}]}, \qquad St = \frac{\omega\delta}{U_\tau} \tag{2}$$

The aerodynamic parameters are defined as $U_\tau = U_\infty\sqrt{C_f/2}$ and $\tau_w = (1/2)\rho U_\infty^2 C_f$, where ρ is the air density and δ is the boundary-layer thickness. The TBL friction coefficient is obtained from the empirical correlation

$$C_f = 0.37\left(\log_{10} Re_y\right)^{-2.584} \tag{3}$$

In this work, all spectral quantities are expressed in terms of frequency f (Hz). Following Miller *et al*. (2012), the Efimtsov spectrum, originally given per rad/s, is converted to PSD per hertz via $S_0(f) = 2\pi\, S_0(2\pi f)$, which yields

$$S_0(f) = \frac{2\pi(0.01\tau_w^2\delta)}{U_\tau\left[1+0.02\left(\frac{2\pi f\delta}{U_\tau}\right)^{2/3}\right]} \tag{4}$$

This form is used together with the Corcos model to construct the cross-spectral density matrix of the wall-pressure field induced by a turbulent boundary layer over the rigid panel.

2.2 STATISTICAL SHAPING FILTER

The target pressure field is generated from uncorrelated white-noise signals $\mathbf{x}$, filtered through a shaping matrix $\mathbf{D}$

$$\mathbf{w} = \mathbf{D}\mathbf{x} \tag{5}$$

This matrix is designed so that the synthesized field exhibits the same cross-spectral density matrix as the target field

$$\mathbf{S}_{ww} = \mathbf{D}\mathbf{D}^{\mathrm{H}} \tag{6}$$

The matrix is obtained via the spectral decomposition of $\mathbf{S}_{ww}$

$$\mathbf{D} = \mathbf{Q}\boldsymbol{\Lambda}^{1/2} \tag{7}$$

where:

$\mathbf{Q}$ contains the eigenvectors and $\boldsymbol{\Lambda}$ the eigenvalues. In this way, $\mathbf{D}$ acts as a statistical shaping filter, responsible for transforming the white-noise signals so that the target field exhibits coherence and spectral properties consistent with the Corcos–Efimtsov model.

2.3 ACOUSTIC CONTROL FILTER

The synthesis is performed using a monopole array with image symmetry. The coupling matrix $\mathbf{A}_{\mathrm{d}}$ relates the signals emitted by the sources to the pressures measured at the observation points. The elements of $\mathbf{A}_{\mathrm{d}}$ are obtained from the acoustic pressure field expression:

$$p(x_j, y_j, z_j, k) = -j\omega\rho_0 \sum_{i=1}^{n} Q_i \left[\frac{e^{jkr_{ij}^-}}{4\pi r_{ij}^-} + \frac{e^{jkr_{ij}^+}}{4\pi r_{ij}^+}\right] \tag{8}$$

where:

Q_i is the volume velocity of the *i*-th monopole source, and r_{ij}^- and r_{ij}^+ are the distances from the real monopole and its image to the observation point (x_j, y_j, z_j), respectively. The spectrum of the generated field is expressed as

$$\mathbf{y} = \mathbf{A}_\mathrm{d}\mathbf{M}\mathbf{x} \tag{9}$$

where:

$\mathbf{M}$ is the control filter matrix, responsible for adjusting the source signals so that the synthesized field reproduces the statistical properties of the target field. The spectral density of the generated field is

$$\mathbf{S}_{yy} = \mathbf{A}_\mathrm{d}\mathbf{M}\mathbf{M}^\mathrm{H}\mathbf{A}_\mathrm{d}^\mathrm{H} \tag{10}$$

2.4 UNREGULARIZED ACOUSTIC SYNTHESIS

The error spectral density is defined as

$$\mathbf{S}_{ee} = \mathbf{A}_\mathrm{d}\mathbf{M}\mathbf{M}^\mathrm{H}\mathbf{A}_\mathrm{d}^\mathrm{H} - \mathbf{A}_\mathrm{d}\mathbf{M}\mathbf{D}^\mathrm{H} - \mathbf{D}\mathbf{M}^\mathrm{H}\mathbf{A}_\mathrm{d}^\mathrm{H} + \mathbf{D}\mathbf{D}^\mathrm{H} \tag{11}$$

Thus, minimizing the mean-square error in the Least Squares sense, $J_e = \mathrm{Tr}[\mathbf{S}_{ee}]$, leads to the optimal control matrix

$$\mathbf{M}_\mathrm{ot} = (\mathbf{A}_\mathrm{d}^\mathrm{H}\mathbf{A}_\mathrm{d})^{-1}\mathbf{A}_\mathrm{d}^\mathrm{H}\mathbf{D} \tag{12}$$

and to the optimal source velocity vector

$$\mathbf{q}_\mathrm{ot}^* = \mathbf{M}_\mathrm{ot}\mathbf{x} \tag{13}$$

and, consequently, to the optimal generated pressure field

$$\mathbf{y}_{\mathrm{ot}} = \mathbf{A}_{\mathrm{d}}\, \mathbf{q}_{\mathrm{ot}}^{*} \tag{14}$$

2.5 REGULARIZED ACOUSTIC SYNTHESIS

To ensure efficiency and stability, the synthesis is regularized by considering only the most efficient ARMs. The modal matrix contains the normalized eigenvectors associated with the dominant eigenvalues of the radiation problem, derived from the model's power-coupling matrix $\mathbf{W}$. The source velocity vector is decomposed in a reduced modal subspace

$$\tilde{\mathbf{q}}^{*} = \tilde{\mathbf{\Psi}}_{\tilde{\mathrm{d}}}\, \tilde{\boldsymbol{\alpha}}^{*} \tag{15}$$

where:

$\tilde{\mathbf{\Psi}}_{\tilde{\mathrm{d}}}$ is the reduced modal matrix formed by the $\tilde{n}$ most efficient ARMs, and $\tilde{\boldsymbol{\alpha}}^{*}$ is the vector of modal contributions. The generated pressure field is then

$$\tilde{\mathbf{y}} = \mathbf{A}_{\mathrm{d}}\, \tilde{\mathbf{\Psi}}_{\tilde{\mathrm{d}}}\, \tilde{\boldsymbol{\alpha}}^{*} \tag{16}$$

The spectral density of the error for the regularized synthesis is

$$\mathbf{S}_{\tilde{e}\tilde{e}} = \mathbf{A}_{\mathrm{d}}\tilde{\mathbf{\Psi}}_{\tilde{\mathrm{d}}}\, \tilde{\mathbf{M}}\tilde{\mathbf{M}}^{\mathrm{H}}\tilde{\mathbf{\Psi}}_{\tilde{\mathrm{d}}}^{\mathrm{H}}\mathbf{A}_{\mathrm{d}}^{\mathrm{H}} - \mathbf{A}_{\mathrm{d}}\tilde{\mathbf{\Psi}}_{\tilde{\mathrm{d}}}\tilde{\mathbf{M}}\mathbf{D}^{\mathrm{H}} - \mathbf{D}\tilde{\mathbf{M}}^{\mathrm{H}}\tilde{\mathbf{\Psi}}_{\tilde{\mathrm{d}}}^{\mathrm{H}}\mathbf{A}_{\mathrm{d}}^{\mathrm{H}} + \mathbf{D}\mathbf{D}^{\mathrm{H}} \tag{17}$$

where:

$\tilde{\mathbf{M}}$ is the reduced control filter matrix. Minimizing the regularized mean-square error, $J_{\tilde{\mathrm{e}}} = \mathrm{Tr}[\mathbf{S}_{\tilde{e}\tilde{e}}]$, leads to the optimal control matrix

$$\tilde{\mathbf{M}}_{\mathrm{ot}} = (\tilde{\mathbf{\Psi}}_{\tilde{\mathrm{d}}}^{\mathrm{H}}\, \mathbf{A}_{\mathrm{d}}^{\mathrm{H}}\, \mathbf{A}_{\mathrm{d}}\, \tilde{\mathbf{\Psi}}_{\tilde{\mathrm{d}}})^{-1}\ \tilde{\mathbf{\Psi}}_{\tilde{\mathrm{d}}}^{\mathrm{H}}\, \mathbf{A}_{\mathrm{d}}^{\mathrm{H}}\, \mathbf{D} \tag{18}$$

which generates the optimal ARMs contributions

$$\tilde{\boldsymbol{\alpha}}_{\mathrm{ot}}^{*} = \tilde{\mathbf{M}}_{\mathrm{ot}}\,\mathbf{x} \tag{19}$$

and, consequently, the regularized pressure field

$$\tilde{\mathbf{y}}_{\mathrm{ot}} = \mathbf{A}_{\mathrm{d}}\,\tilde{\boldsymbol{\Psi}}_{\tilde{\mathrm{d}}}\;\tilde{\boldsymbol{\alpha}}_{\mathrm{ot}}^{*} \tag{20}$$

2.6 CONTROL METRICS

The synthesized acoustic field, which corresponds statistically to the TBL-induced wall-pressure field, was evaluated using three complementary metrics that quantify spectral fidelity, spatial coherence, and physical feasibility of the reconstruction. These metrics are defined and examined for both the unregularized case and the ARMs-regularized case.

2.6.1 Normalized mean-square error

This metric quantifies the overall spectral fidelity, representing the portion of the target field's total energy $\mathbf{S}_{ww}$ that lies outside the synthesis space.

$$\hat{J}_{e} = \frac{\mathrm{Tr}[\left(\mathbf{I}-\mathbf{A}_{\mathrm{d}}\mathbf{A}_{\mathrm{d}}^{\dagger}\right)\mathbf{S}_{ww}]}{\mathrm{Tr}[\mathbf{S}_{ww}]} \tag{21}$$

$$\hat{J}_{\tilde{\mathrm{e}}} = \frac{\mathrm{Tr}\left[\left(\mathbf{I}-\mathbf{A}_{\mathrm{d}}\tilde{\boldsymbol{\Psi}}_{\tilde{\mathrm{d}}}\left(\mathbf{A}_{\mathrm{d}}\tilde{\boldsymbol{\Psi}}_{\tilde{\mathrm{d}}}\right)^{\dagger}\right)\mathbf{S}_{ww}\right]}{\mathrm{Tr}[\mathbf{S}_{ww}]} \tag{22}$$

where:

$\mathbf{A}_{\mathrm{d}}{}^{\dagger}$ and $\left(\mathbf{A}_{\mathrm{d}}\tilde{\boldsymbol{\Psi}}_{\tilde{\mathrm{d}}}\right)^{\dagger}$ are the pseudoinverses of the matrices $\mathbf{A}_{\mathrm{d}}$ and $\mathbf{A}_{\mathrm{d}}\tilde{\boldsymbol{\Psi}}_{\tilde{\mathrm{d}}}$, respectively. Criterion: $\hat{J}_{e} < -10\ \mathrm{dB}$ indicates that less than 10% of the total energy of the target field lies outside the synthesis space, indicating good fidelity.

2.6.2 Residual error

This metric indicates how well the spatial structure of the target field is preserved by the synthesized field, not only in terms of total energy (as in $\hat{J}_e$) but also in how that energy is distributed spatially across the measurement points.

$$\varepsilon_{\mathbf{y}} = \frac{\|\mathbf{C}_{ww} - \mathbf{C}_{yy}\|_{\mathrm{F}}}{\|\mathbf{C}_{ww}\|_{\mathrm{F}}} \tag{23}$$

$$\varepsilon_{\tilde{\mathbf{y}}} = \frac{\|\mathbf{C}_{ww} - \mathbf{C}_{\tilde{y}\tilde{y}}\|_{\mathrm{F}}}{\|\mathbf{C}_{ww}\|_{\mathrm{F}}} \tag{24}$$

where:

$\|\cdot\|_{\mathrm{F}}$ denotes the Frobenius norm, $\mathbf{C}_{ww}$, $\mathbf{C}_{yy}$ and $\mathbf{C}_{\tilde{y}\tilde{y}}$ are the spatial correlation matrices of the target and generated pressure fields.

The construction of $\mathbf{C}_{yy}$, based on the spectral density matrix $\mathbf{S}_{yy}$, is detailed in Bravo & Maury (2006). Criterion: $\varepsilon_{\mathbf{y}} < -1\,\mathrm{dB}$ indicates acceptable spatial reproduction. This means that the residual error contains less than 20% of the energy of the original correlation matrix, reflecting good preservation of the spatial structure.

2.6.3 Root-mean-square source velocity norm

This metric quantifies the total effort of the sources (monopoles) in reproducing the desired field, i.e., it indicates how much energy the sources need to radiate to generate the target pressure field.

$$\| \overline{\mathbf{q}^{*2}} \| = \sqrt{\mathrm{Tr}\left[\mathbf{A}_{\mathrm{d}}^{\dagger}\mathbf{D}\mathbf{D}^{\mathrm{H}}\left(\mathbf{A}_{\mathrm{d}}^{\dagger}\right)^{\mathrm{H}}\right]} \tag{25}$$

$$\| \overline{\tilde{\mathbf{q}}^{*2}} \| = \sqrt{\mathrm{Tr}\left[\tilde{\mathbf{\Psi}}_{\tilde{\mathrm{d}}}\left(\mathbf{A}_{\mathrm{d}}\tilde{\mathbf{\Psi}}_{\tilde{\mathrm{d}}}\right)^{\dagger}\mathbf{D}\mathbf{D}^{\mathrm{H}}\left(\left(\mathbf{A}_{\mathrm{d}}\tilde{\mathbf{\Psi}}_{\tilde{\mathrm{d}}}\right)^{\dagger}\right)^{\mathrm{H}}\tilde{\mathbf{\Psi}}_{\tilde{\mathrm{d}}}^{\mathrm{H}}\right]} \quad (26)$$

High values suggest a risk of saturation, instability, or nonlinearity, sensitivity to noise, and poor conditioning of the transfer matrix. Low values — achieved via ARMs — indicate a more efficient and stable synthesis, with reduced physical and numerical effort.

3 NUMERICAL SYNTHESIS RESULTS

Numerical simulations targeted acoustic synthesis up to $f_{max} = 1\,\mathrm{kHz}$ over a rigid, acoustically reflecting panel of dimensions $0.328\mathrm{m}\,(\mathrm{spanwise}, x) \times 0.768\mathrm{m}\,(\mathrm{streamwise}, y)$. A planar array of monopole sources, coextensive with the panel, was used together with image sources to enforce a Neumann boundary at the panel plane. The source grid comprised $n_x \times n_y = 24 \times 10 = 240$ monopoles with spacings $s_x = 0.01426\,\mathrm{m}$ and $s_y = 0.08533\,\mathrm{m}$; these spacings satisfy the acoustic grating-lobe condition $\Delta_s \leq c/(2f_{max}) = 0.1715\,\mathrm{m}$ and also the spanwise correlation sampling rule of 2.1 sources per L_x, i.e., $s_x \lesssim L_x/2.1$. In the more restrictive case $\mathrm{Mach}\ 0.7$, $L_x = \alpha_x U_c/(2\pi f_{max}) \approx 0.0321\,\mathrm{m}$ so $L_x/2.1 \approx 0.0153\,\mathrm{m}$ and $s_x = 0.01426\,\mathrm{m}$ complies; similarly, $L_y/2.1 \approx 0.102\,\mathrm{m}$ and $s_y = 0.08533\,\mathrm{m}$ complies. The microphone array comprised $m_x \times m_y = 49 \times 23 = 1127$ equally spaced sensors located $0.002\,\mathrm{m}$ above the panel, with spacings $d_x = 0.006833\,\mathrm{m}$ and $d_y = 0.03491\,\mathrm{m}$. Aliasing limits derived from Corcos coherence and the convective Nyquist criterion provide comfortable margins up to $1\,\mathrm{kHz}$: for $\mathrm{Mach}\ 0.7$, $f_{\mathrm{lim},x} = 2349\,\mathrm{Hz}$ and $f_{\mathrm{lim},y} = 2407\,\mathrm{Hz}$ $(\mathrm{coherence\ only} = 3065\,\mathrm{Hz}, \mathrm{Nyquist} = 2407\,\mathrm{Hz})$; for $\mathrm{Mach}\ 0.9$, $f_{\mathrm{lim},x} = 3020\,\mathrm{Hz}$ and $f_{\mathrm{lim},y} = 3095\,\mathrm{Hz}$ $(\mathrm{coherence\ only} = 3941\,\mathrm{Hz}, \mathrm{Nyquist} = 3095\,\mathrm{Hz})$. The monopole plane was placed $0.1\mathrm{m}$ from the panel with coincident centers. Control performance was evaluated using unregularized least squares (LS) and LS regularized with Acoustic Radiation Modes (ARMs), employing a 60-mode subset (far-field and near-field ARMs) selected from the 240 available by radiation efficiency.

Table 1. Approximate aerodynamic parameters.

Parameter	Mach 0.7	Mach 0.9
Free-stream velocity U_∞ (m/s)	240.1	308.7
Shear stress τ_w (N/m^2)	66.5623	106.0907
Friction velocity U_τ (m/s)	7.4169	9.3637
Boundary layer thickness δ (m)	0.0336	0.0326

Source: the authors (2025)

Table 1 presents the approximate aerodynamic parameters of the flow, for two Mach numbers, over a rigid flat panel, which were used in the numerical simulations. The parameters were estimated assuming air at 20℃ and 1 atm, with air density $\rho_0 = 1.21\ \mathrm{kg/m^3}$, sound speed $c = 343\ \mathrm{m/s}$, and kinematic viscosity $\nu = 1.5111 \times 10^{-5}\ \mathrm{m^2/s}$.

Figure 1. Normalized mean-square error as a function of frequency for two Mach numbers.

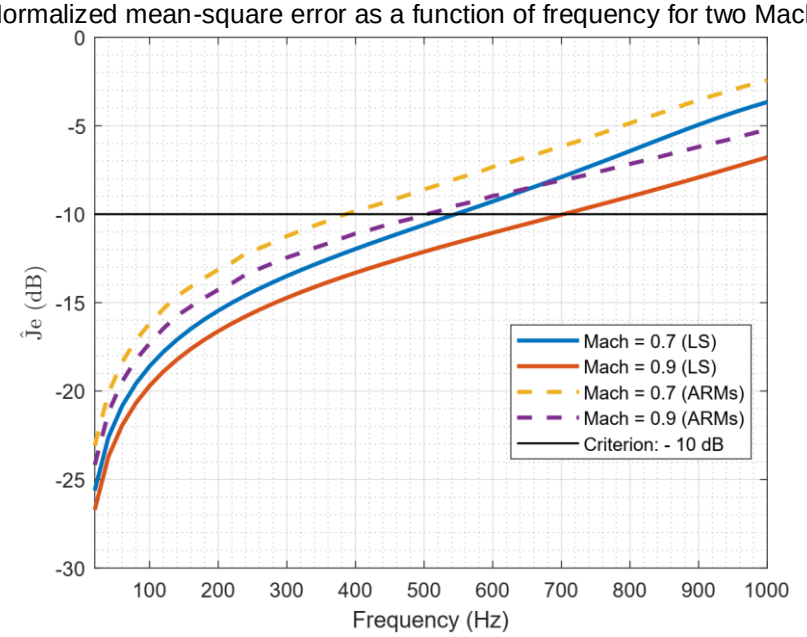

Source: the authors (2025).

Fig. 1 presents the behavior of the normalized mean-square error as a function of frequency, a metric that quantifies the overall spectral fidelity between the synthesized pressure field and the target field modeled using the combined Corcos–Efimtsov formulation. The LS method exhibits lower error levels across most of the frequency range, remaining below $-10\ \mathrm{dB}$ over the band and approaching the limit near $1\ \mathrm{kHz}$. This indicates that less than 10% of the total

energy of the target field lies outside the synthesis space, demonstrating excellent statistical agreement.

This performance directly results from exploiting all available degrees of freedom in the monopole array, allowing the LS method to fully project the target field onto the radiation space represented by the coupling matrix $\mathbf{A}_{\mathrm{d}}$. Consequently, the amplitudes and phases of the sources are optimally adjusted, ensuring that the radiated field accurately reproduces the spectral energy distribution of the turbulent boundary layer.

In contrast, the ARMs-regularized solution exhibits higher $\hat{J}_e$ values, particularly at high frequencies. This difference stems from the modal reduction applied — only the 60 most efficient radiation modes were retained out of the 240 available. Modal truncation constrains the system's ability to reproduce higher-order spatial components, which are associated with short-scale fluctuations and become increasingly relevant in the high-frequency region. As a result, part of the target-field energy is not captured, increasing the synthesis error.

Overall, Fig. 1 highlights the trade-off between fidelity and stability: while the LS approach provides maximum spectral accuracy at the expense of higher source effort and numerical sensitivity, the ARMs regularization sacrifices some fidelity in favor of robustness and practical feasibility.

Fig. 2 shows the residual error versus frequency, a metric that emphasizes preservation of the spatial coherence of the wall-pressure field. Unlike $\hat{J}_e$, which gauges global energy deviation, $\varepsilon_{\mathbf{y}}$ compares the correlation structures of the target field ($\mathbf{C}_{ww}$) and the synthesized field ($\mathbf{C}_{yy}$), thus indicating how well phase–amplitude relationships across the surface are reproduced. The curves include Mach 0.7 and 0.9 for both LS and ARMs, with the $-1\ \mathrm{dB}$ acceptability line shown for reference.

Figure 2. Residual error as a function of frequency for two Mach numbers.

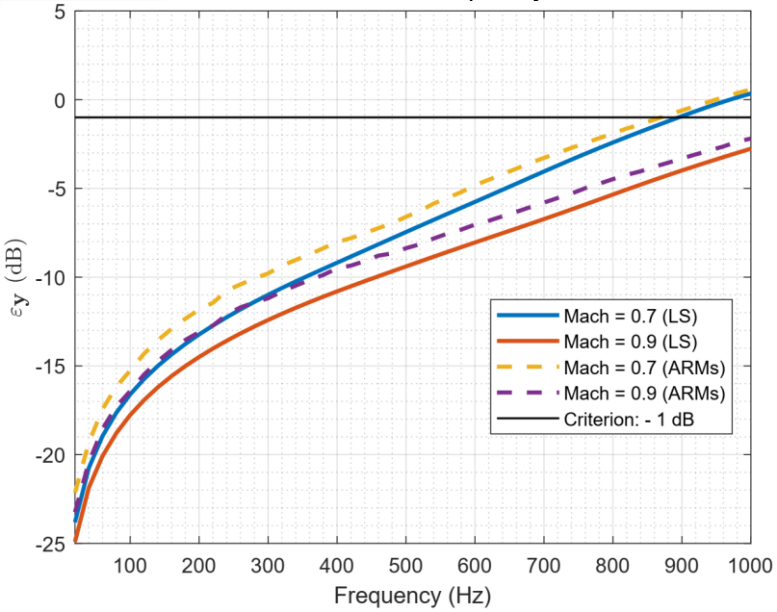

Source: the authors (2025).

Consistent with Fig. 1, the LS solution yields the lowest $\varepsilon_{\mathbf{y}}$ across the band, typically remaining at or below $-1\,\mathrm{dB}$, with Mach 0.7 marginally outperforming Mach 0.9 near the upper frequencies. This indicates that LS preserves the convective coherence pattern while matching mean energy, benefiting from access to the full radiation space.

ARMs regularization leads to higher $\varepsilon_{\mathbf{y}}$, especially toward $900 - 1000\,\mathrm{Hz}$, where some curves approach or slightly exceed the $-1\,\mathrm{dB}$ threshold. The increase reflects modal truncation: limiting the subspace attenuates short-scale components and underestimates transverse coherence. Overall, Fig. 2 illustrates the expected trade-off: LS maximizes coherence fidelity at the cost of higher source effort, whereas ARMs provide a more robust, physically stable solution with some loss of fine spatial detail—appropriate for practical implementations.

Figure 3. Spatial correlation structures for the theoretical reproduction of a TBL field at Mach 0.9 (top), for the synthesized field without regularization using the LS method (middle), and with ARMs regularization (bottom).

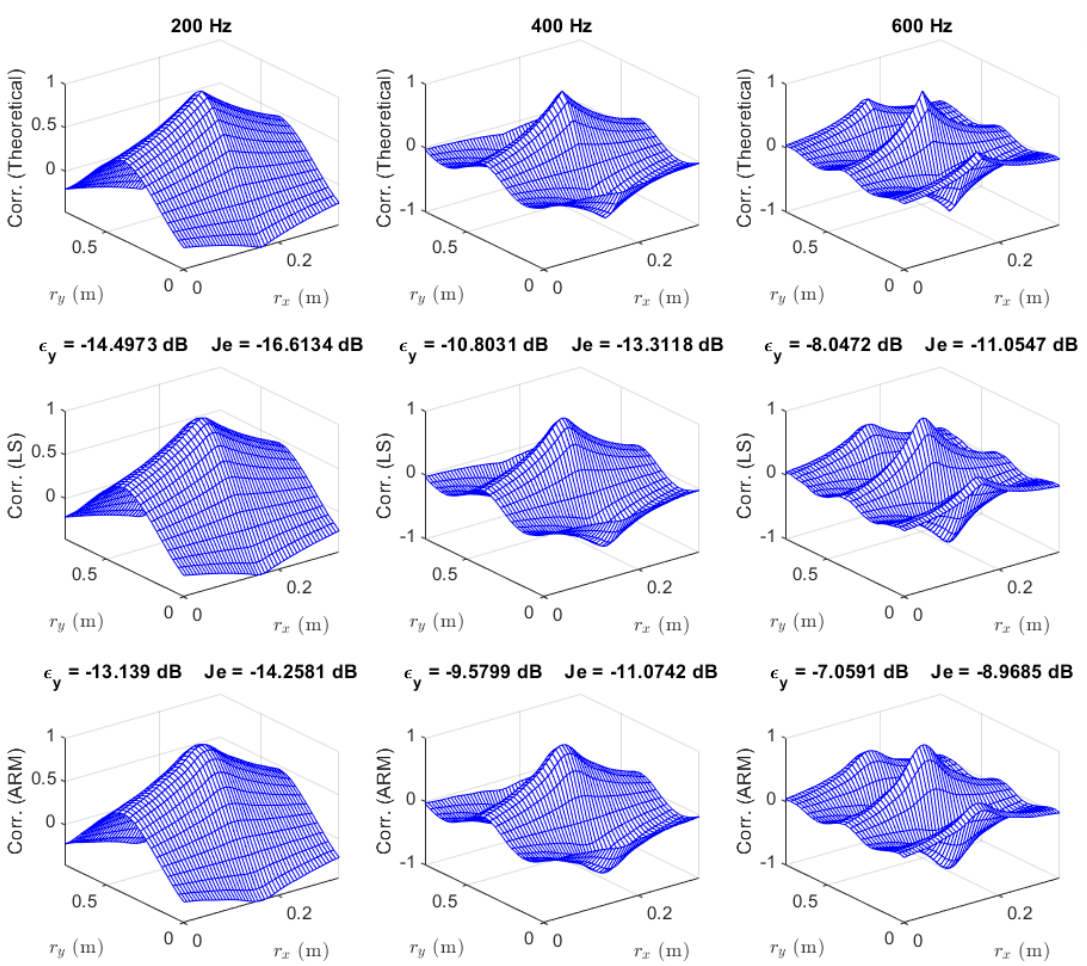

Source: the authors (2025).

Fig. 3 compares the spatial correlation structures of wall-pressure fluctuations generated by the turbulent boundary layer (TBL), highlighting how the theoretical coherence patterns are reproduced by the synthesis methods. The top row shows the theoretical field predicted by the Corcos model. At 200 Hz, the correlation pattern extends over a wide, coherent region associated with large eddies convecting along the surface. As frequency increases to 400 Hz and 600 Hz, the contours become more oscillatory and fragmented, reflecting shorter correlation lengths and phase reversals linked to smaller turbulent structures.

The middle row shows the LS-synthesized fields. The agreement with the theoretical model is excellent across the band. At 200 Hz, the synthesized and theoretical fields are nearly identical ($\hat{J}_e = -16.6$ dB, $\varepsilon_{\mathbf{y}} = -14.5$ dB), and even at

$400\ \mathrm{Hz}$ and $600\ \mathrm{Hz}$ the amplitude and phase structures remain well preserved ($\hat{J}_e = -13.3\ \mathrm{dB}, -11.1\ \mathrm{dB}; \varepsilon_{\mathbf{y}} = -10.8\ \mathrm{dB}, -8.0\ \mathrm{dB}$). These results confirm that LS effectively captures the convective topology of the TBL pressure field, preserving spatial coherence and the anisotropy imposed by the mean flow.

The ARMs-based synthesis (bottom row) reproduces the general correlation pattern but exhibits gradual smoothing at higher frequencies. Retaining only the 60 most efficient radiation modes limits the reconstruction of short-wavelength components, especially in the spanwise direction. Fine-scale coherence features are partially filtered out, slightly increasing the errors ($\hat{J}_e = -14.3\ \mathrm{dB}$ to $-9\ \mathrm{dB}$; $\varepsilon_{\mathbf{y}} = -13.1\ \mathrm{dB}$ to $-7\ \mathrm{dB}$) but improving numerical stability and reducing source effort. This truncation acts as a physically meaningful regularization, suppressing near-singular modes that add little to the radiated energy yet amplify instability.

Figure 4. Root-mean-square velocity norm as a function of frequency for two Mach numbers.

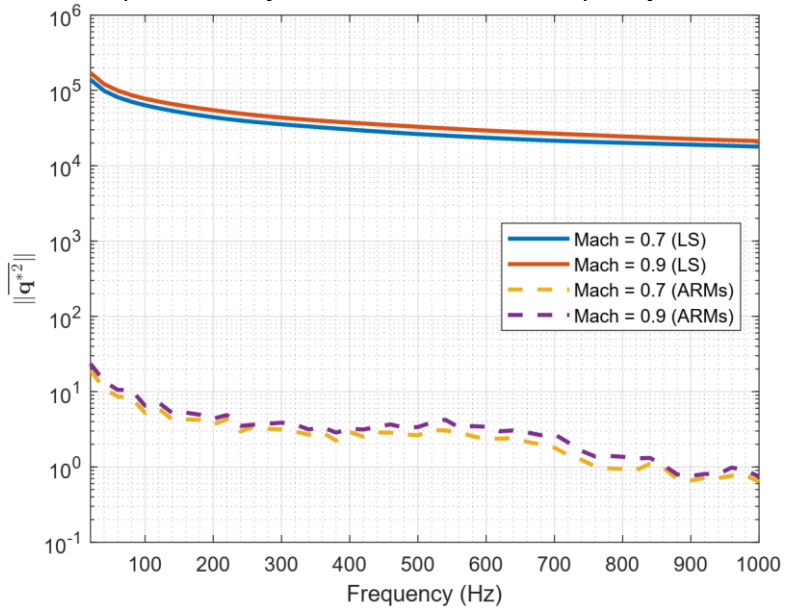

Source: the authors (2025).

Fig. 4 presents the root-mean-square velocity norm of the sources, which quantifies the physical and energetic effort required to synthesize the target field. This parameter represents the total power radiated by the array and is directly linked to the conditioning of the inverse problem and the experimental feasibility.

The LS method exhibits very high $\| \overline{\mathbf{q}^{*2}} \|$ values—ranging roughly from 10^4 up to 10^5 over the band—indicating source amplitudes that are impractical for experimental implementation. This behavior results from the ill-conditioned nature of the coupling matrix ($\mathbf{A}_\mathrm{d}$): by minimizing the synthesis error without regularization, the LS solution amplifies components associated with small singular values, yielding unstable and energetically unbalanced source distributions. Consequently, although LS ensures the highest statistical fidelity (i.e., the lowest $\hat{J}_e$ and $\varepsilon_\mathbf{y}$), its energetic cost renders physical implementation unfeasible.

In contrast, the ARMs method reduces source effort by several orders of magnitude, with typical values between 10^0 and 10^1. This efficiency stems from modal regularization, which confines the synthesis to the most efficient radiation modes—those converting source energy into sound most effectively. By excluding ill-conditioned and inefficient modes, ARMs stabilizes the inverse problem and yields a more uniform, physically coherent distribution of source amplitudes.

Therefore, the LS method provides maximum fidelity, but at the cost of high energetic effort and numerical instability. In contrast, the ARMs method yields a more stable, efficient, and experimentally feasible solution, with only a slight loss of fidelity. This balance between statistical accuracy and practical feasibility represents the core objective of the proposed methodology.

To establish the frequency range over which the ARMs-regularized synthesis remains statistically valid, a cut-off frequency was defined based on the residual-error criterion ($\varepsilon_\mathbf{y} < -1\ \mathrm{dB}$). This threshold ensures that at least $\sim 80\%$ of the spatial-correlation energy of the target field is preserved, corresponding to good reproduction of the coherence structure characteristic of wall-pressure fluctuations induced by turbulent boundary layers. Although the normalized mean-square error criterion ($\hat{J}_e < -10\ \mathrm{dB}$) also indicates acceptable global spectral fidelity, it is less sensitive to spatial-phase deviations and thus less physically representative of the synthesized field. The residual-error-based definition of f_c therefore provides a more stringent and physically meaningful limit, identifying the highest frequency at which the ARMs approach can accurately reproduce both the amplitude and the convective coherence of the target pressure field; beyond

this frequency, modal truncation progressively smooths the field and reduces coherence even if the overall energy level remains approximately correct.

Table 2. Estimated cut-off frequencies for ARMs-regularized synthesis (target f_{max} = 1 kHz)

Mach	$\tilde{n}$ (ARMs)	$f_{c,\hat{J}_e}$ [Hz]	f_{c,ε_y} [Hz]	Observation
0.7	40	310	820	Stable through mid frequencies; does not reach 1 kHz in residual.
0.9	40	400	1060	Gradual coherence loss above ~ 900 Hz; residual meets the 1 kHz target with a small margin.
0.7	60	390	860	Spatial coherence preserved up to ~ 860 Hz; still below 1 kHz for Mach = 0.7.
0.9	60	510	1110	Robust performance; residual comfortably exceeds 1 kHz; $\hat{J}_e$ advances to ~ 500 Hz.
0.7	80	440	880	Near full-band reproduction; residual approaches but does not reach 1 kHz.
0.9	80	560	1130	Upper-band extension with a comfortable margin > 1 kHz in residual; $\hat{J}_e$ improved without instability.
0.7	240 (LS)	550	890	Unregularized LS raises $f_{c,\hat{J}_e}$, but residual gains are modest; higher conditioning/effort risk.
0.9	240 (LS)	700	1150	Residual well above 1 kHz; $\hat{J}_e$ remains <1 kHz; watch conditioning and control effort.

Source: the authors (2025)

Table 2 summarizes the estimated cut-off frequencies for two Mach numbers (0.7 and 0.9) and three ARMs truncations ($\tilde{n} = 40, 60, 80$), including the unregularized LS reference ($\tilde{n} = 240$). The values were obtained from the frequency-domain curves of $\hat{J}_e\,(f)$ and $\varepsilon_y\,(f)$. For each case, f_{c,ε_y} denotes the first frequency at which the residual error exceeds -1 dB, while $f_{c,\hat{J}_e}$ corresponds to the -10 dB limit. As expected, retaining more ARMs extends the coherent bandwidth, enabling accurate reproduction of spatial coherence at higher frequencies. Consistent with the table, for Mach 0.9 the residual cut-off exceeds 1 kHz even with $\tilde{n} = 40$, while for Mach 0.7 it remains below 1 kHz up to $\tilde{n} = 80$. Thus, higher-speed flows—whose wall-pressure spectra contain more high-frequency energy—benefit from increased modal retention. Insufficient truncation leads to coherence degradation at high frequencies, underscoring the importance of appropriate ARMs-based regularization.

4 CONCLUSIONS

The results confirm that the proposed methodology can statistically reproduce random wall-pressure fields representative of turbulent boundary layers (TBL) by using a planar array of monopole sources together with image sources to impose a Neumann boundary at the panel plane. Although monopoles are idealizations, their analytical tractability and well-characterized radiation enable a clear physical interpretation of the synthesis process and an efficient numerical implementation.

The unregularized least-squares (LS) formulation achieved the highest statistical fidelity, accurately reproducing both the spectral energy distribution and the spatial coherence of the Corcos–Efimtsov target fields (Mach 0.7 and 0.9, up to $1\ \mathrm{kHz}$). However, the required source effort was prohibitively large, reflecting the ill-conditioning of the coupling operator and limiting experimental feasibility.

Acoustic Radiation Mode (ARM) regularization stabilized the inversion and reduced energetic demand by several orders of magnitude while preserving the dominant coherence and spectral features of the target. The moderate loss of fidelity observed at the highest frequencies is attributable to modal truncation, which confines the solution space to the most efficient radiating modes, and nevertheless, the ARM-based synthesis remained physically consistent, stable, and experimentally realizable.

Overall, the study establishes a coherent framework for controlled reproduction of TBL-induced wall-pressure fields that balances accuracy, robustness, and computational efficiency. The approach provides a solid basis for experimental validation and for future extensions to non-uniform source layouts, structural/acoustic coupling, and near-field synthesis.

REFERENCES

BRAVO, T.; MAURY, C. The experimental synthesis of random pressure fields: methodology. *The Journal of the Acoustical Society of America*, **120**(5), 2702–2711, 2006.

CORCOS, G. M. The structure of the turbulent pressure field in boundary-layer flows. *Journal of Fluid Mechanics*, **18**(3), 353–378, 1964.

EFIMTSOV, B. M. Characteristics of the field of turbulent wall pressure fluctuations at large Reynolds numbers. *Soviet Physics Acoustics*, **28**, 289–292, 1982.

ELLIOTT, S. J.; MAURY, C.; GARDONIO, P. The synthesis of spatially correlated random pressure fields. *The Journal of the Acoustical Society of America*, **117**(3), 1186–1201, 2005.

MAURY, C.; BRAVO, T. The experimental synthesis of random pressure fields: practical feasibility. *The Journal of the Acoustical Society of America*, **120**(5), 2712–2723, 2006.

MERLO, C. A. Synthesis of the diffuse random pressure field using active and reactive radiation modes. *Contemporary Journal*, **3**(11), 20849–20872, 2023.

MERLO, C. A.; PASQUAL, A. M.; MEDEIROS, E. B. Sound field synthesis on flat panels using a planar source array controlled by its active and reactive radiation modes. *Acta Acustica united with Acustica*, **105**(1), 139–151, 2019.

MILLER, T. S.; GALLMAN, J. M.; MOELLER, M. J. Review of turbulent boundary layer models for acoustic analysis. *Journal of Aircraft*, **49**(6), 1739–1754, 2012.

PASQUAL, A. M.; ARRUDA, J. R. F.; HERZOG, P. Application of acoustic radiation modes in the directivity control by a spherical loudspeaker array. *Acta Acustica united with Acustica*, **96**(1), 32–42, 2010.

Revista CADERNO PEDAGÓGICO

ISSN: 1983-0882

Qualis CAPES 2017-2020: A2

DECLARAÇÃO

Caderno Pedagógico, ISSN 1983-0882, declara para os devidos fins, que o artigo intitulado **Acoustic synthesis of random wall-pressure fields from turbulent boundary layers using monopole arrays and acoustic radiation modes** de autoria de Clinton André Merlo, Otávio Lage Dias, Rogério Fernandes Brito, foi publicado no v.22, n.13, de 2025.

A revista é on-line, e os artigos podem ser encontrados ao acessar o link:

https://ojs.studiespublicacoes.com.br/ojs/index.php/cadped/issue/view/163

DOI: https://doi.org/10.54033/cadpedv22n13-024

Por ser a expressão da verdade, firmamos a presente declaração.

Curitiba, 4 novembro 2025

Equipe Editorial